

Metal Nanowire Arrays by Electrodeposition

Erich C. Walter,^[a] Michael P. Zach,^[b] Frédéric Favier,^[c] Benjamin J. Murray,^[a] Koji Inazu,^[d] John C. Hemminger,^[a] and Reginald M. Penner*^[a]

We describe two related methods for preparing arrays of nanowires composed of molybdenum, copper, nickel, gold, and palladium. Nanowires were obtained by selectively electrodepositing either a metal oxide or a metal at the step edges present on the basal plane of highly oriented pyrolytic graphite (HOPG) electrodes. If a metal oxide was electrodeposited, then nanowires of the parent metal were obtained by reduction at elevated temperature in hydrogen. The resulting nanowires were organized in parallel arrays of 100–1000 wires. These nanowires were long (some >500 μm), poly-

crystalline, and approximately hemicylindrical in cross-section. The nanowire arrays prepared by electrodeposition were also “portable”: After embedding the nanowires in a polymer or cyanoacrylate film, arrays of nanowires could be lifted off the graphite surface thereby facilitating the incorporation of metal nanowire arrays into devices such as sensors.

KEYWORDS:

electrochemistry · electrodeposition · nanowires · metals · sensors

Recent studies of the electrical and magnetic properties of metal wires smaller than 100 nm in diameter (“nanowires”) have revealed a variety of fascinating properties. For example, gold nanowires smaller than the mean free path of an electron (50 nm) exhibit a depressed conductivity caused by classical boundary scattering.^[1] The conductance and yield strength of atomic-scale gold wires are both quantized.^[2–11] The shot noise in metal nanowires is suppressed^[12] while the thermoelectric figure of merit is enhanced.^[13–15] The conductivity of gold nanowires immersed in liquids is reduced by the presence in the liquid of adsorbates such as thiols.^[16–18] These studies suggest that metal nanowires might form the basis for chemical sensors. Bismuth nanowires can have a magnetoresistance (r/r_0) of up to 44 000%.^[19–22] Finally, arrays of fractured palladium nanowires can function as hydrogen gas sensors.^[23, 24]

Collectively, these exciting results provide motivation for the development of new methods for preparing metal nanowires. In particular, methods are required for preparing long nanowires (millimeters or centimeters in length), with control of the wire diameter, composition, and microstructure. The synthetic method should produce nanowires that are predisposed to manipulation, if possible. We have developed two related methods that meet some of these criteria. These methods are described here.

Results and Discussion.

We have discovered^[23–28] that metal nanowires can be obtained by selectively electrodepositing metals or conductive metal oxides at the step edges present on a HOPG surface. It is useful to put this discovery into historical perspective. The idea of using step edges to template the growth of nanowires, sometimes called “step edge decoration”, is approximately ten years old. Physical vapor deposition (PVD) experiments conducted in the early 1990s revealed that step edge decoration could be employed to produce continuous wirelike nanostructures; see

for example refs. [29–34]. During the last five years surface scientists working in ultrahigh vacuum, especially the groups of Himpfel^[30, 35–37] and Kern,^[38–41] have established the importance of step edge decoration as a means for preparing metal nanowires on vicinal single crystal surfaces using PVD. Metal nanowires of monoatomic width have been prepared,^[38, 40] control of nanowire “width” and wire spacing has been demonstrated,^[37] and long metal nanowires that are many microns in length have been created.^[38] However it has not been demonstrated that these PVD-deposited nanowires can be removed from the surfaces on which they are deposited.

Literature precedents also exist for the growth of nanowires on HOPG surfaces. Myrick^[42] was the first to show that step edges on graphite could be selectively decorated via the electrodeposition of the conducting polymer polypyrrole. McDermott and co-workers^[43] identified conditions for the chemical vapor deposition of platinum on HOPG that lead to the formation of nanowires along step edges.

[a] Prof. R. M. Penner, E. C. Walter, B. J. Murray, Prof. J. C. Hemminger
Department of Chemistry
University of California—Irvine
Irvine, CA 92697-2025 (USA)
Fax: (+1) 949-842-3168
E-mail: rmpenner@uci.edu

[b] Dr. M. P. Zach
Department of Earth and Planetary Science
University of California—Berkeley
Berkeley, CA 94720-4767 (USA)

[c] Dr. F. Favier
Laboratoire des Agrégats Moléculaires et Matériaux Inorganiques (LAMMI),
CNRS
Université Montpellier II
34095 Montpellier Cedex 05 (France)

[d] Dr. K. Inazu
Department of Environmental Chemistry & Engineering,
Tokyo Institute of Technology
4259 Nagatsuta, Midori-ku, Yokohama 226-8502 (Japan)

Two ESED Strategies

Electrochemical step-edge decoration (ESED) can be implemented in two different ways to obtain metal nanowire arrays. These two methods are shown schematically in Figure 1. The more complicated of the two methods (Figure 1a) involves the

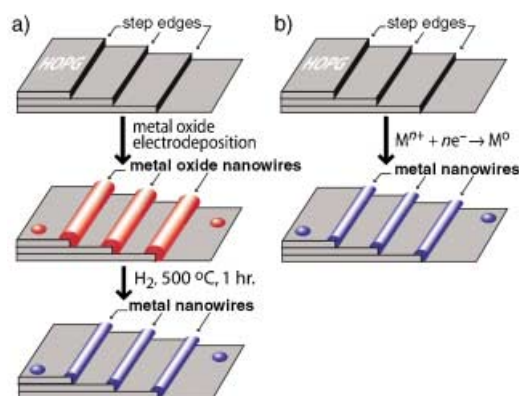
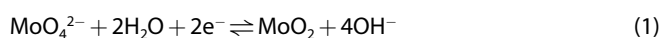


Figure 1. Two methods for preparing metal nanowires based on electrochemical step-edge decoration. a) Electrodeposition of an electronically conductive metal oxide nanowires followed by reduction in hydrogen. b) Direct electrodeposition of metal nanowires.

electrodeposition of metal oxide nanowires followed by reduction in hydrogen to obtain metal nanowires.^[26–28] Most of our work to date has involved the electrodeposition of nanowires composed of MoO₂ and the reduction of these to Mo⁰. However we have confirmed that nanowires of other conductive metal oxides, including Cu₂O and Fe₂O₃, may also be electrodeposited. If these metal oxide nanowires are already conductive, what is the motivation for reducing these to obtain metal nanowires? The most compelling reason is that the metal nanowires have improved ductility and resistance to breakage. Metal oxide nanowires do not withstand the mechanical stresses associated with our process for transferring wires (described below).^[28] The second method (Figure 1 b), involving the direct electrodeposition of metal nanowires at step edges,^[23–25, 27] is conceptually simpler but it is more difficult to successfully employ in the laboratory. We describe both of these methods in greater detail below.

Electrochemically Decorating Step Edges on Graphite with Metal Oxides

The cyclic voltammogram of a graphite surface in a solution containing MoO₄²⁻ is shown in Figure 2. As the potential is scanned negatively from +0.1 to –1.25 V versus a saturated calomel reference electrode (V_{SCE}), two reductions are observed. An onset for the MoO₂ deposition is seen at approximately –0.60 V_{SCE}. Reaction (1) is responsible for MoO₂ deposition.



Also seen at –1.10 V_{SCE} is current associated with the onset for H₂ evolution. In this solution, MoO₂ can be electrodeposited at

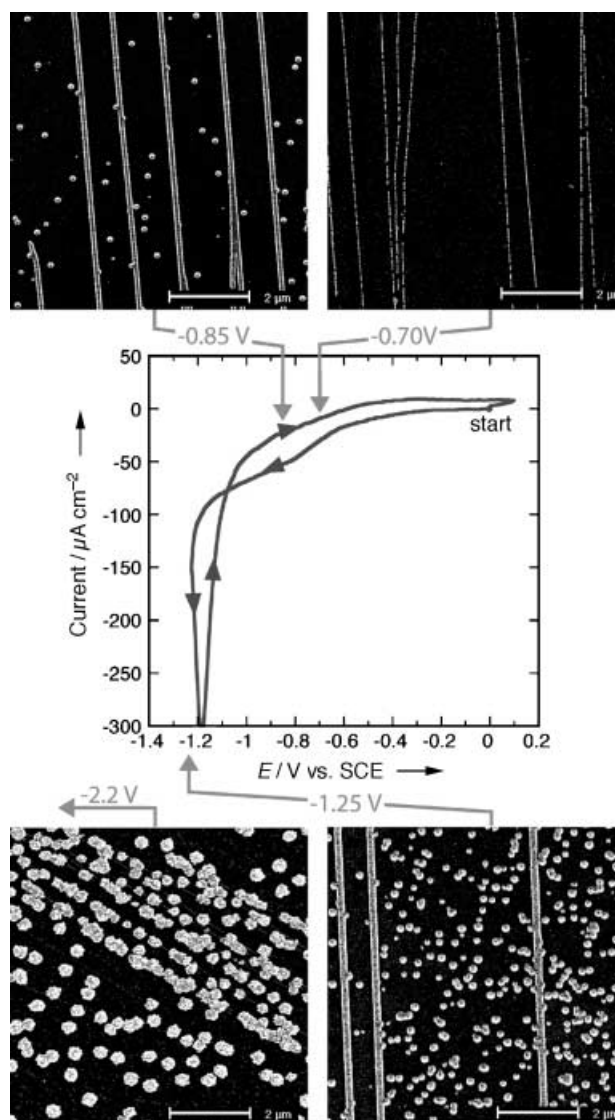


Figure 2. Cyclic voltammogram at 20 mV s⁻¹ for an HOPG working electrode in an aqueous plating solution containing 1 mM Na₂MoO₄, 1.0 M NaCl, and 1.0 M NH₄Cl, adjusted to pH 8.5 with the addition of aqueous NH₃. Also shown are SEM images (scale bars 2 μm) showing HOPG surfaces after the deposition of MoO₂ for 256 s (or 1024 s at –0.70 V_{SCE}). The plating solution in these experiments was 7 mM Na₂MoO₄, 1.0 M NaCl, 1.0 M NH₄Cl, pH 8.5. These images demonstrate that MoO₂ nucleation becomes less selective for step edges as the deposition potential is decreased from –0.70 to –2.2 V versus SCE.

any potential negative of –0.60 V_{SCE}, however the selectivity of nucleation, and therefore the distribution of MoO₂ on the graphite surface, changes dramatically as the deposition overpotential is increased. The evolution of the selectivity of nucleation can be seen clearly in the four SEM images shown in Figure 2. At a deposition potential of –0.70 V_{SCE}, MoO₂ nucleates exclusively at step edges on the graphite surface, however a deposition time of more than 15 min is required to obtain the 40 nm diameter nanowires. The other three SEM images shown in Figure 2 were obtained after just 256 s (4.5 min) of deposition. At –0.85 V_{SCE}, MoO₂ nucleates with a high degree of selectivity at step edges but a small number of particles (less than 1 μm⁻²) are also formed on terraces. Nanowires 150 nm in

diameter are obtained. At even more negative potentials of -2.2 and $-1.25 V_{SCE}$, the number of particles seen on terraces increases dramatically. At $-2.2 V_{SCE}$, in fact, nanowire growth at steps is disrupted by vigorous H_2 evolution^[44] and large MoO_2 particles are seen both at steps and on terraces. We have concluded that a growth potential in the range from -0.75 to $-0.90 V_{SCE}$ is close to optimum for MoO_2 nanowire growth in these plating solutions.^[26] Within this voltage range, the nucleation density along step edges is greater than $20 \mu m^{-1}$ and hemispherical MoO_2 particles, located next to one another on a step, rapidly coalesce to form continuous nanowires that are many microns in length. This "coalescence point" coincides with a nanowire diameter of approximately $10-15 nm$.^[26, 28]

The current associated with MoO_2 electrodeposition decreases with time for the first $20-150 s$ of growth, after which it stabilizes at 20 to $50 \mu A cm^{-2}$ and becomes invariant with time. Both the time required to attain steady state, and the magnitude of the steady-state current depend on the deposition potential. For example, in one particular sequence of experiments conducted using the same graphite crystal, $E_{dep} = -0.70 V_{SCE}$ yielded a steady-state deposition current of $25 \mu A cm^{-2}$ within $20 s$ whereas $E_{dep} = -0.85 V_{SCE}$ produced a steady-state current of $45 \mu A cm^{-2}$ at $150 s$. Since the radius of the MoO_2 nanowires increases from $5-10 nm$ to more than $100 nm$ within $100 s$ (even for $E_{dep} = -0.70 V_{SCE}$), the current, controlled either kinetically by deposition^[45] or by diffusion of MoO_4^{2-} ,^[46-48] should increase continuously during nanowire growth. However because of the cylindrical nanowire geometry, this current increase can be virtually imperceptible over the time scale investigated here, because in cylindrical diffusion the current depends only on the length of the wire, the logarithm of time and the logarithm of the wire radius.^[46-48]

The pseudo-steady-state deposition current I_{dep} leads to a simple expression for the time-dependent nanowire radius, $r(t)$, given by Equation (1), where I_{dep} is the deposition current density, t_{dep} is the deposition duration, V_m is the molar volume of the deposited material ($19.8 cm^3 mol^{-1}$ for MoO_2), n is the number of electrons transferred for the deposition of each MoO_2 unit, and L is the total length of nanowires present within a $1.0 cm^2$ area of the graphite surface.^[26, 28]

$$r(t) = \sqrt{\frac{2 I_{dep} t_{dep} V_m}{\pi n F L}} \quad (1)$$

The radius $\propto (\text{time})^{1/2}$ functionality predicted by Equation (1) is seen experimentally. For example, a plot of nanowire diameter versus $t_{dep}^{1/2}$ for nanowires prepared at $-0.9 V_{SCE}$ is shown centered in Figure 3. Also shown in Figure 3 are SEMs of MoO_2 nanowires prepared at $-0.85 V$ from a $1.0 mM MoO_4^{2-}$ solution using t_{dep} values ranging from 8 to $256 s$. Nanowires varying in diameter from 40 to $700 nm$ were obtained. Thus, MoO_2 nanowires of a predetermined diameter can be obtained once the slope of the wire diameter versus $t_{dep}^{1/2}$ plot is known.

It is apparent from the SEM images of Figure 3 that MoO_2 nanowires have excellent intra- and interwire diameter uniformity. A high degree of uniformity is present in MoO_2 nanowires that are just $50 nm$ in diameter, and uniformity is maintained as nanowires are grown to $1.0 \mu m$ in diameter. This "convergent

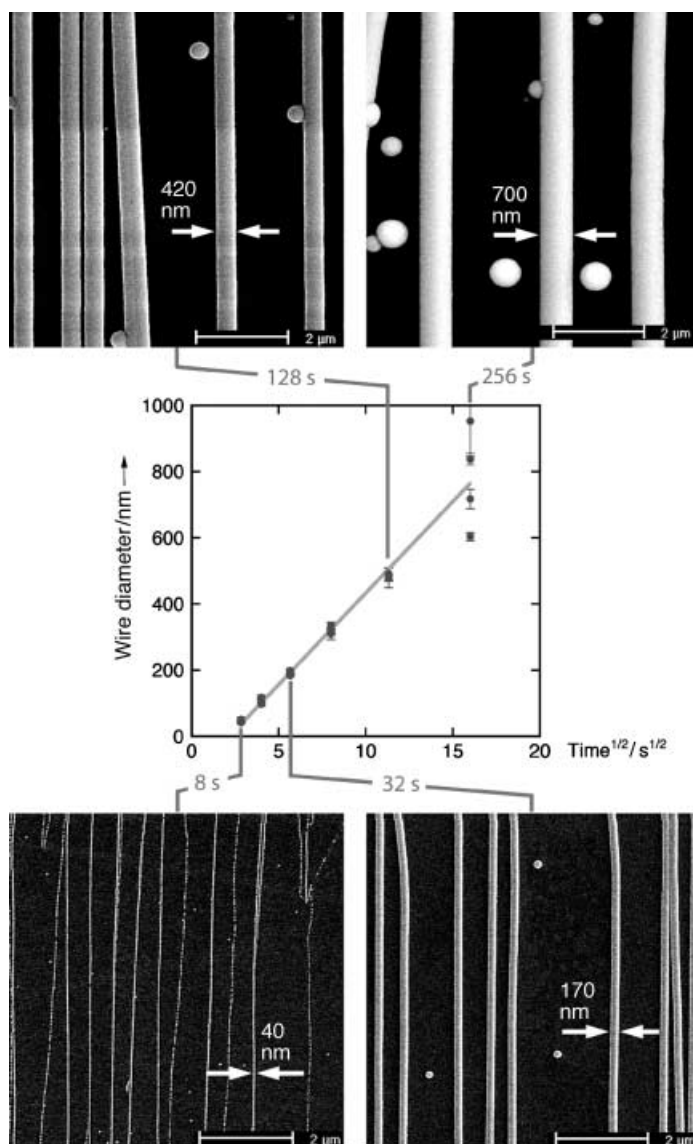


Figure 3. Plot of the MoO_2 nanowire diameter as a function of the square root of the deposition time. The growth conditions in this experiment were $E_{dep} = -0.90 V_{SCE}$, $0.16 mM Na_2MoO_4$, $1.0 M NaCl$, $1.0 M NH_4Cl$, pH 8.5. The linearity of this plot is consistent with the predictions of Equation (1). Also shown are SEM images (scale bars $2 \mu m$) showing HOPG surfaces after the deposition of MoO_2 for various durations as indicated.

growth" behavior is a remarkable property of the nanowire electrodeposition process. We believe the origin of this behavior derives from the growth law of Equation (1). As shown graphically in Figure 4, the growth of a rough nanowire in accordance with the predictions of Equation (1) results in smoothing of the nanowire surface because $dr/dt \propto r^{-1}$. As we shall see, convergent growth in accordance with Equation (1) is observed for a variety of metals and with both of the nanowire growth methods shown in Figure 1.

The high-magnification SEM images of Figure 3 hint at the parallel organization of nanowires on the graphite surface. This organization is made clearer in the low-magnification SEM image of Figure 5a. This image shows the center of a large grain on the graphite basal plane after the deposition of MoO_2 nanowires.

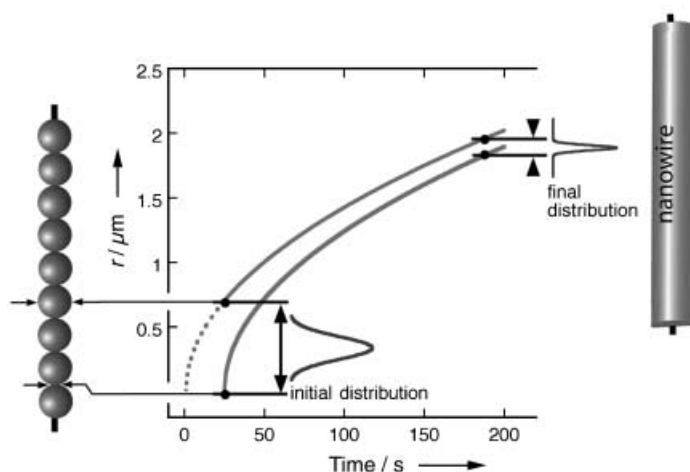


Figure 4. Schematic diagram depicting the effect of the $r \propto t^{1/2}$ growth law, Equation (1), on the smoothness of a nanowire. The rate of radial growth dr/dt is inversely proportional to the nanowire radius. This means that constrictions along the axis of a rough nanowire increase in radius faster than bulges on the same wire. The net effect, obtained after a period of constant current growth, is a smoothing of the nanowire surface. Reprinted with permission from ref. [26], copyright 2002 American Chemical Society.

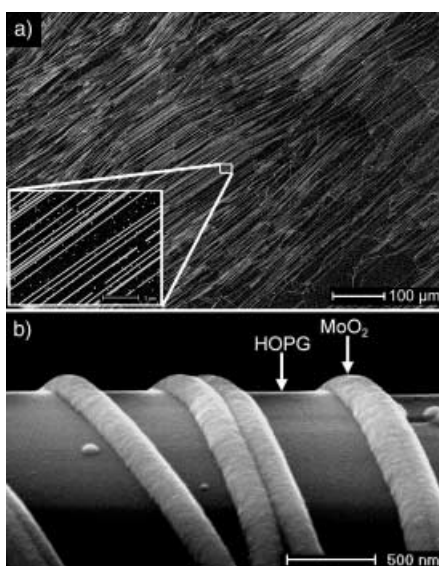


Figure 5. a) Low magnification SEM image (scale bar $100 \mu\text{m}$, inset $2 \mu\text{m}$) of an HOPG surface after the deposition of MoO_2 nanowires. The step edges present within individual grains on the HOPG surface are oriented parallel to one another. Terraces with widths of $50 - 500 \text{ nm}$ on average separate steps from one another. b) Perspective view (scale bar $500 \mu\text{m}$) of MoO_2 nanowires showing hemicylindrical geometry. Reprinted with permission from ref. [26], copyright 2002 American Chemical Society.

This image clearly shows that within the confines of the grain, step edges are organized into parallel arrays. These arrays can contain thousands of individual steps, and these steps can be continuous for distances of up to 1 mm . Because these attributes are transferred to the MoO_2 nanowires that nucleate on these step edges, nanowires with lengths of more than $100 \mu\text{m}$ are routinely obtained in these experiments.^[26, 28] These nanowires are hemicylindrical, as shown in the side-on SEM image of

Figure 5 b. This hemicylindrical geometry is a reflection of the geometry of diffusion to the step edges responsible for templating nanowire growth.

We identify the deposited molybdenum oxide in these experiments as MoO_2 using X-ray photoelectron spectroscopy (XPS). A second oxide of molybdenum, MoO_3 , can also be electrodeposited from MoO_4^{2-} -containing solutions. XPS spectra (not shown) of electrodeposited “ MoO_2 ” nanowires exhibit a Mo $3d_{5/2}$ peak at 229.8 eV that compares with literature values for MoO_2 and MoO_3 of 229.2 and 232.7 eV , respectively. We conclude that the deposited material is predominantly MoO_2 .

Conversion of MoO_2 Nanowires to Mo^0

Molybdenum nanowires are obtained from MoO_2 nanowires by reduction in hydrogen.^[26, 28] At 500°C , this reduction requires approximately 1 h for nanowires up to 300 nm in diameter. Because the molar volume of Mo^0 is 9.4 mol cm^{-3} and that of MoO_2 is 19.8 mol cm^{-3} , nanowires shrink during the reduction process. The shrinkage in diameter of $19 - 25\%$ is shown for the reduction of one particular MoO_2 nanowire in the SEM images of Figure 6. The completeness of the reduction process is confirmed by electron diffraction, X-ray fluorescence, and XPS analysis of the nanowires^[26] (data not shown). After reduction at $500 - 650^\circ\text{C}$ for 1 h , the Mo $3d_{5/2}$ binding energy was 228.1 eV —exactly the expected binding energy for molybdenum metal.

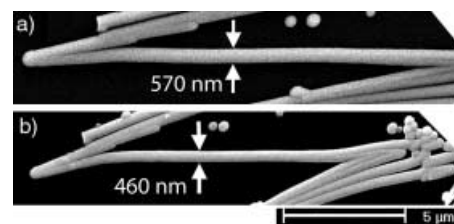


Figure 6. SEM micrographs (scale bar $5 \mu\text{m}$) of a particular electrodeposited MoO_2 nanowire a) before and b) after reduction at 500°C for 1 h . The observed shrinkage in wire diameter is due to the difference in molar unit volume per Mo atom between MoO_2 and Mo^0 .

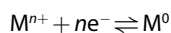
While MoO_2 nanowires shrink during the reduction process, the shape of the bends in these wires was hardly affected, as shown in Figure 6. This shape invariance during reduction is surprising, as both the volume and the surface free energy of the wire are altered as it undergoes conversion from MoO_2 to molybdenum metal.

We have demonstrated^[28] that individual molybdenum nanowires that are $300 - 400 \text{ nm}$ in diameter have a conductivity approximately an order of magnitude lower than molybdenum metal. The conductivity of nanowires in air, however, decreases as a function of time because the surface of the nanowire is oxidized to insulating MoO_3 . The composition of this oxide was verified from XPS.^[26, 28]

“Direct” Metal Nanowire Electrodeposition by ESED.

The strategy of Figure 1 a cannot be applied to the preparation of platinum, palladium, and gold nanowires because for these

metals thermodynamically stable and conductive bulk oxides do not exist. Instead, it is necessary to obtain nanowires by the direct step-edge selective electrodeposition (Figure 1 b) of the metal M according to Reaction (2).



Experimentally, however, it is more difficult to achieve nanowire growth using this “direct electrodeposition” strategy. The problem is that a suitable nanowire growth overpotential does not exist: An overpotential negative enough to produce nanowires of M at steps ($20\text{--}50\ \mu\text{m}^{-1}$) causes progressive nucleation (a nucleation density that increases with time) on the surrounding terraces. At this overpotential, a metal film is obtained. If a lower overpotential is employed, the nucleation density at steps is too low ($2\text{--}5\ \mu\text{m}^{-1}$) to yield nanowires. In a metal oxide electrodeposition experiment, in contrast, it is generally possible to locate a potential that produces a high nucleation density at step edges, a low nucleation density on terraces (namely, appreciable step-edge selectivity), and a significant growth rate for nanowires at steps. For MoO_2 , for example, potentials in the range from -0.7 to $-0.9\ V_{\text{SCE}}$ satisfy these three criteria, as discussed previously.

The solution to this problem is shown in Figures 7 and 8. In order to obtain nanowires by direct electrodeposition of metal,

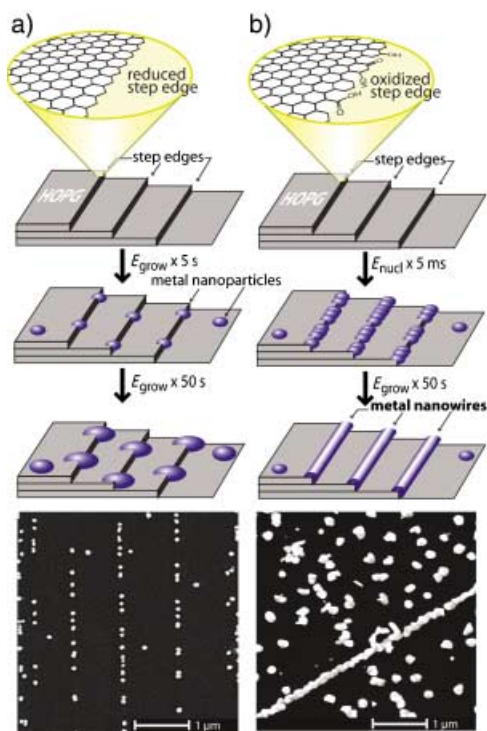


Figure 7. The step-edge selectivity of metal electrodeposition is enhanced by preoxidizing the graphite surface and by applying a large-amplitude short-duration nucleation pulse. a) When this is not done, the nucleation density along steps is low and metal nanowires can not be obtained. The SEM image shows gold nuclei on HOPG prepared by a single, potentiostatic pulse. b) Preoxidation and the application of a nucleation pulse increase the nucleation density at steps and permits metal nanowires to be directly electrodeposited. However a large number of particles are also obtained in these experiments. The SEM image shows a gold nanowire and gold particles prepared using the synthesis conditions indicated in Table 1.

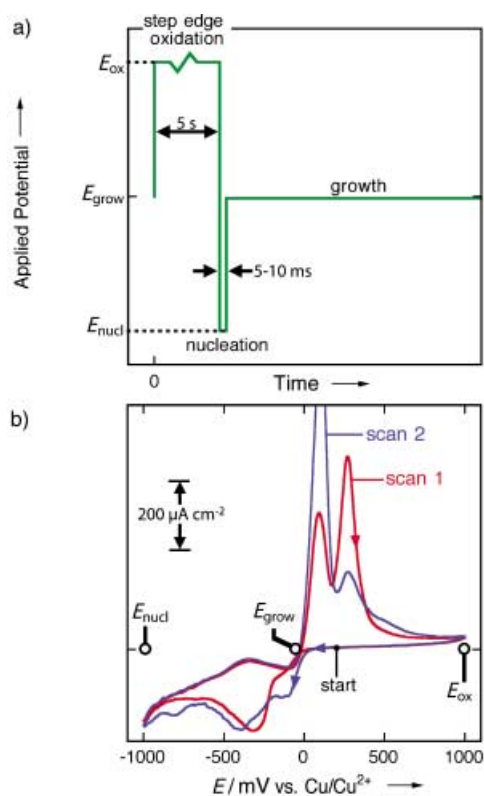


Figure 8. a) Triple voltage pulse used to prepare metal nanowires in this study. b) Cyclic voltammograms of a copper plating solution at an HOPG electrode showing the values for E_{ox} , E_{nucl} , and E_{grow} typically used for the preparation of copper nanowires. The solution was aqueous $2.0\ \text{mM}\ \text{CuSO}_4 \cdot 5\text{H}_2\text{O}$, $0.1\ \text{M}\ \text{Na}_2\text{SO}_4$. Two oxidation waves seen at $+100\ \text{mV}_{\text{SCE}}$ and $+350\ \text{mV}_{\text{SCE}}$ are assigned to copper stripping ($+100\ \text{mV}_{\text{SCE}}$) and oxidation of Cu^0 to CuO ($+350\ \text{mV}_{\text{SCE}}$). Reprinted with permission from ref. [25], copyright 2002 American Chemical Society.

the procedure for nanowire growth must be altered in three ways: First, the step edges must be chemically differentiated from terraces by oxidizing them electrochemically. This is accomplished in the metal plating solution by oxidation for 5 s at $+0.8\ V_{\text{SCE}}$. Secondly, the nucleation density at step edges must be increased by applying a very short ($<20\ \text{ms}$), very negative ($\eta \approx -1.0\ \text{V}$) nucleation pulse to initiate nanowire growth. Thirdly, after this nucleation pulse is applied, subsequent growth is carried out using the smallest possible overpotential ($\eta < -50\ \text{mV}$). This three-pulse scheme is shown together with the cyclic voltammogram for a copper plating solution in Figure 8.

This strategy works well for the four metals we have investigated so far: copper, nickel, gold, and palladium. Optimized plating parameters required for nanowire growth are summarized in Table 1. SEM images of copper nanowires with diameters ranging from 70 to 340 nm are shown in Figure 9. After the nucleation voltage pulse is applied, nanowire growth at E_{grow} is characterized by a constant current I_{dep} , exactly as seen for MoO_2 electrodeposition and the same growth law, Equation (1), therefore applies.

In contrast to the smooth MoO_2 nanowires prepared on graphite by potentiostatic electrodeposition,^[26, 28] individual metal grains—with diameters approximately equal to the

Metal	Plating Solution ^[a]	E_{ox} [V]	t_{ox} [s]	E_{nuc} [V]	t_{nuc} [s]	E_{grow} [V _{SCE}]
molybdenum	1.0–10 mM Na ₂ MoO ₄ 1.0 M NaCl 1.0 M NH ₄ Cl pH = 8.5	–	–	–	–	–0.70 to –0.85
nickel	1.0 mM NiSO ₄ ·6H ₂ O 0.1 M Na ₂ SO ₄	0.8	5	–1.0	0.005	–0.900
copper	2.0 mM CuSO ₄ ·5H ₂ O 0.1 M Na ₂ SO ₄	0.8	5	–0.8	0.005	–0.005
gold	1.0 mM AuCl ₃ 0.1 M NaCl	0.8	5	–0.8	0.010	+0.560
palladium	1.0 mM PdCl ₂ , 0.1 M HCl or 1.0 mM Pd(NO ₃) ₂ , 0.1 M HClO ₄	0.8	5	–0.8	0.010	+0.300

[a] All solutions are aqueous; all potentials referenced to SCE.

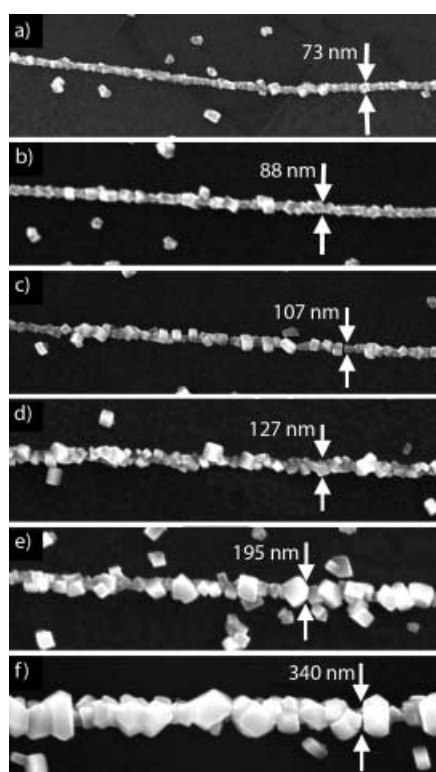


Figure 9. SEM images of copper nanowires. These nanowires were electro-deposited from the solution indicated in Table 1, using $E_{\text{nuc}} = -800 \text{ mV}_{\text{SCE}}$ and $E_{\text{grow}} = -5 \text{ mV}_{\text{SCE}}$. The growth times employed in each experiment were a) 120, b) 180, c) 300, d) 600, e) 900, and f) 2700 s. Reprinted with permission from ref. [25], copyright 2002 American Chemical Society.

diameters of the nanowires—are clearly visible in the SEM images of Figure 9. Palladium, nickel, and gold nanowires prepared using this triple-pulse method are visually very similar.^[23, 24] The granular morphology of these nanowires contrasts with the smooth surfaces seen for amorphous MoO₂ nanowires^[26, 28] and it is instructive to ask why these two types of nanowires are so different. We believe that larger grains are formed with the triple-pulse method because nucleation at step edges can occur only during the 5–10 ms nucleation pulse. After the nucleation pulse is over, the metal nuclei increase in

diameter but the growth potential is too low to permit the formation of new metal nuclei. In contrast, the formation of new metal oxide nuclei appears to continue during the electro-deposition of metal oxide nanowires. Metal particles that have nucleated on terraces can be seen in all of the SEM images shown in Figure 9, and are also seen on surfaces after the preparation of palladium, gold, and nickel nanowires.^[23, 24] Nucleation at terraces occurs at E_{nuc} albeit with a lower efficiency than nucleation at oxidized step edges. Consequently, we have found that some parallel growth of particles on terraces is inevitable in these experiments. Like MoO₂ nanowire growth, a time-invariant deposition current is observed during the growth phase of nickel, copper, gold, and palladium nanowires. Based on Equation (1), we expect to observe a linear increase of nanowire diameter with $t_{\text{dep}}^{1/2}$ for these metals exactly as seen for MoO₂ nanowire growth. As shown in Figure 10, this expectation is realized for three of these metals—copper, nickel, and gold—but the plot for palladium nanowires is nonlinear for reasons that are as yet unclear.

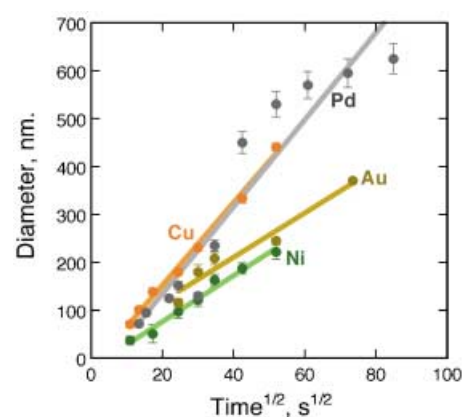


Figure 10. Nanowire diameter versus $t_{\text{dep}}^{1/2}$ for the growth of nanowires composed of four metals as indicated. Each series of experiments for a particular metal were performed using a single graphite crystal in order to limit the variation in the step edge density from experiment to experiment, see Equation (1). This crystal was cleaved before each experiment to expose a fresh and clean graphite surface. Error bars for each data point are twice the standard deviation for the mean particle diameter.

Preparation of Portable Nanowire Arrays

In order to prepare a device that exploits the conductivity of metal nanowires, they must be transferred from the graphite surface onto the surface of an insulator. Our procedure for lifting nanowire arrays off a graphite electrode is shown in Figure 11.^[23] Briefly, the graphite surface on which the metal nanowires are located is pressed against a droplet of an adhesive. The identity of the adhesive depends on the specific application, and we have used epoxy, cyanoacrylate, and polystyrene solutions for this purpose. This adhesive covers the area where nanowires have been deposited. After the adhesive has hardened or dried (usually overnight), the graphite is removed but the vast majority of the nanowires remain embedded at the surface of the adhesive. In this process, we are aided by the mechanically resiliency of metal nanowires, and by the fact that these structures adhere weakly to the step edges on which they nucleate. The parallel ordering of nanowires, seen for example in Figure 5a, is retained during transfer. Thus, parallel arrays of metal nanowires can be located on the surface of a cyanoacrylate film and metal contacts applied to the ends of these nanowire arrays, as shown in the SEM image of Figure 12. It is apparent from this image the palladium nanoparticles are also transferred together with the nanowires, however these particles cannot contribute to the conduction across the nanowire array and so their presence is not detrimental. We have recently demonstrated^[23, 24] that arrays of transferred palladium nanowires can be used to prepare a hydrogen gas sensor having several unique attributes.^[23]

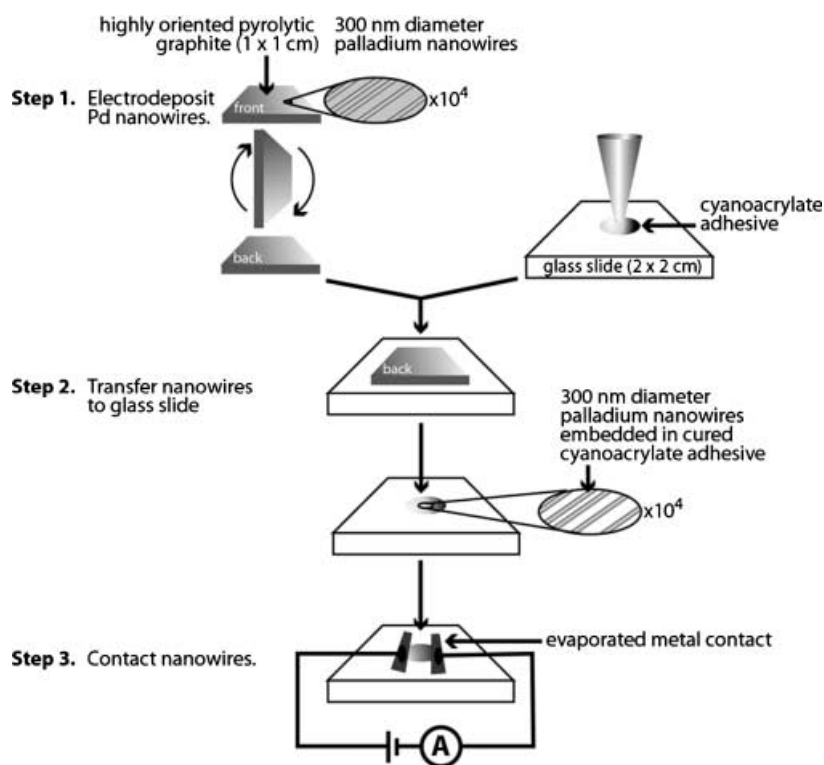


Figure 11. Procedure for transferring metal nanowire arrays from the HOPG surface to another surface. Reprinted with permission from ref. [23], copyright 2002 American Chemical Society.

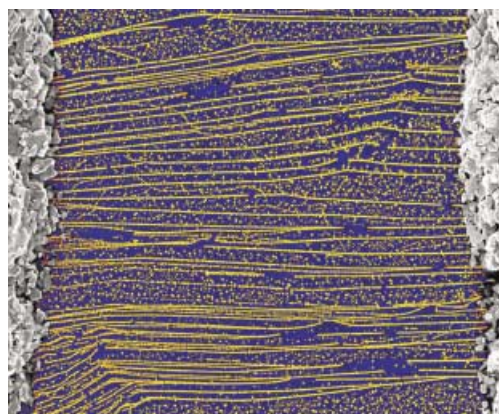


Figure 12. SEM image of an array of palladium nanowires (yellow) embedded in cyanoacrylate (blue) supported on a glass slide. This nanowire array, which was a functioning hydrogen sensor, is contacted at the far left and right with silver paint (gray). The total width of this image is 300 μm ; the diameter of each wire is approximately 200 nm. Reprinted with permission from ref. [23], copyright 2002 American Chemical Society.

Conclusions

Metal oxides such as MoO_2 and metals such as copper, nickel, gold, and palladium can be selectively electrodeposited at the step edges present on the basal plane of HOPG. Electrodeposited nanowires of metal oxides can be converted into metal nanowires by reduction in hydrogen at high temperature. This electrochemical step-edge decoration (ESED) provides a new and very general method for preparing metal nanowires that possess important attributes including adjustability of the diameter, excellent dimensional uniformity, strength, and lengths of more than 500 μm . Metal nanowires prepared by ESED can be removed from the graphite surface by embedding them in a film of an adhesive. During this removal process, metal nanowires retain the parallel ordering that is characteristic of the ordering of step edges on the graphite surface. After this transfer process is complete, arrays of metal nanowires can be electrically contacted with a conductive paint for further electrical characterization, or for the preparation of devices such as chemical sensors. We hope that the unique aspects of ESED nanowire growth can be exploited to prepare a variety of interesting and useful nanometer-scale devices in the future.

Experimental Methods.

Nanowire Electrodeposition: All electrodeposition experiments were carried out in glass, one-compartment, three-electrode cells. The composition of the metal plating solutions are provided in Table 1. These solutions were prepared using Nanopure water ($\rho > 17 \text{ M}\Omega$), and were purged with N_2 before each experiment. All potentials are referenced to a saturated calomel reference electrode. Nanowire electrodeposition experiments were carried out on the basal plane surface of ZYB-grade

HOPG crystals (Advanced Ceramics). The basal plane surface of a HOPG crystal was cleaved using adhesive tape immediately prior to use. The potential pulses required for nanowire growth were applied using an potentiostat/galvanostat (EG&G model 273, 263, or Versastat). After deposition was complete, the graphite working electrode was removed from the plating solution, rinsed with water, and air-dried prior to characterization using SEM.

Reduction of Metal Oxides and Removal from HOPG: The reduction of metal oxide nanowires to the parent metal was effected by heating the graphite working electrode in a tube furnace at 500 to 650 °C under an atmosphere of pure H₂ or a H₂/N₂ 10%/90% for 1–3 h depending on the wire diameter. Reduced metal nanowires were lifted off of the HOPG surface by casting a polystyrene film using one drop of a 20 wt.% polystyrene (from a Styrofoam cup) solution in toluene (Fischer ACS grade). After drying in air, the resulting film with embedded nanowires was peeled off the graphite surface using a forceps. Free-standing molybdenum nanowires could be released from the polystyrene film by stretching this film by a few percent.

X-ray Photoelectron Spectroscopy: XPS was carried out using an ESCALAB MKII photoelectron spectrometer (VG Scientific). The ESCALAB MKII is based on an ultrahigh vacuum (UHV) system consisting of three separately pumped, interconnected chambers (for sample preparation, fast sample entry, and spectroscopy). The fast entry chamber allowed rapid sample transfer from air to UHV pressures (base pressures during analysis were in the low-to-mid 10⁻¹⁰ Torr range). The XPS experiments were performed in the spectroscopy chamber using a standard Mg anode X-ray source (Mg_{Kα} line at 1253.6 eV) and a 150 mm hemispherical electron energy analyzer. The spectra presented here were obtained using an analyzer pass energy of 20 eV. Under these conditions the spectrometer energy resolution was ~0.8 eV. Samples were prepared by supporting the graphite surface, upon which the nanowires were prepared, on a copper sample holder using conductive colloidal silver paste (Ted Pella).

Microscopy: SEM was carried out on uncoated samples using a microscope (FEG-30XL, Philips) equipped with EDX elemental analysis capabilities. TEM was carried using a CM-20 (Philips) machine. HOPG flakes with attached nanowires were transferred to uncoated copper grids (uncoated copper, Ted Pella) for analysis using TEM. These flakes were obtained by mechanically scraping the HOPG surface with the grid.

This work was funded by the National Science Foundation through contract CHE-0111557. We also gratefully acknowledge an American Chemical Society, Division of Analytical Chemistry Fellowship to M.P.Z., sponsored by Merck & Co. K.I. and J.C.H. acknowledge funding support from the Department of Energy through contract DE-FG03-96ER45576. R.M.P. acknowledges the financial support of the A. P. Sloan Foundation Fellowship and the Camille and Henry Dreyfus Foundation. Discussions with Prof. Christian Amatore on the issue of MoO₂ electrodeposition current transients are gratefully acknowledged. Finally, we thank Dr. Art Moore of Advanced Ceramics for many donations of graphite.

- [1] C. Durkan, M. E. Welland, *Phys. Rev. B* **2000**, *61*, 14215.
- [2] J. M. Krans, C. J. Muller, I. K. Yanson, T. C. M. Govaert, R. Hesper, J. M. Vanruitenbeek, *Phys. Rev. B* **1993**, *48*, 14721.
- [3] J. M. Krans, J. M. Vanruitenbeek, V. V. Fisun, I. K. Yanson, L. J. Dejongh, *Nature* **1995**, *375*, 767.
- [4] C. J. Muller, J. M. Krans, T. N. Todorov, M. A. Reed, *Phys. Rev. B* **1996**, *53*, 1022.

- [5] J. I. Pascual, J. Mendez, J. Gomezherrero, A. M. Baro, N. Garcia, U. Landman, W. D. Luedtke, E. N. Bogachek, H. P. Cheng, *J. Vac. Sci. Technol. B* **1995**, *13*, 1280.
- [6] J. I. Pascual, J. Méndez, J. Gómez-Herrero, A. M. Baró, N. García, U. Landman, W. D. Luedtke, E. N. Bogachek, H. P. Cheng, *Science* **1995**, *267*, 1793.
- [7] J. I. Pascual, J. Méndez, J. Gómez-Herrero, A. M. Baró, N. García, V. T. Binh, *Phys. Rev. Lett.* **1993**, *71*, 1852.
- [8] J. L. Costa-Krämer, N. García, H. Olin, *Phys. Rev. Lett.* **1997**, *78*, 4990.
- [9] J. L. Costa-Krämer, N. García, P. García-Mochales, P. A. Serena, M. I. Marqués, A. Correia, *Phys. Rev. B* **1997**, *55*, 5416.
- [10] J. L. Costa-Krämer, N. García, H. Olin, *Phys. Rev. B* **1997**, *55*, 12910.
- [11] J. L. Costa-Krämer, *Phys. Rev. B* **1997**, *55*, R4875.
- [12] M. Henny, S. Oberholzer, C. Strunk, C. Schönenberger, *Phys. Rev. B* **1999**, *59*, 2871.
- [13] O. Rabina, Y. M. Lin, M. S. Dresselhaus, *App. Phys. Lett.* **2001**, *79*, 81.
- [14] Y. M. Lin, X. Z. Sun, M. S. Dresselhaus, *Phys. Rev. B* **2000**, *62*, 4610.
- [15] X. Sun, Z. Zhang, M. S. Dresselhaus, *App. Phys. Lett.* **1999**, *74*, 4005.
- [16] A. Bogozi, O. Lam, H. X. He, C. Z. Li, N. J. Tao, L. A. Nagahara, I. Amlani, R. Tsui, *J. Am. Chem. Soc.* **2001**, *123*, 4585.
- [17] C. Z. Li, H. X. He, A. Bogozi, J. S. Bunch, N. J. Tao, *App. Phys. Lett.* **2000**, *76*, 1333.
- [18] C. Z. Li, H. X. He, A. Bogozi, J. S. Bunch, N. J. Tao, *App. Phys. Lett.* **2000**, *76*, 1333.
- [19] F. Y. Yang, G. J. Strijkers, K. Hong, D. H. Reich, P. C. Searson, C. L. Chien, *J. Appl. Phys.* **2001**, *89*, 7206.
- [20] C. L. Chien, F. Y. Yang, K. Liu, D. H. Reich, P. C. Searson, *J. Appl. Phys.* **2000**, *87*, 4659.
- [21] K. M. Hong, F. Y. Yang, K. Liu, D. H. Reich, P. C. Searson, C. L. Chien, F. F. Balakirev, G. S. Boebinger, *J. Appl. Phys.* **1999**, *85*, 6184.
- [22] K. Liu, C. L. Chien, P. C. Searson, Y. Z. Kui, *IEEE Trans. Magn.* **1998**, *34*, 1093.
- [23] E. C. Walter, F. Favier, R. M. Penner, *Anal. Chem.* **2002**, *74*, 1546.
- [24] F. Favier, E. C. Walter, M. P. Zach, T. Benter, R. M. Penner, *Science* **2001**, *293*, 2227.
- [25] E. C. Walter, B. Murray, F. Favier, G. Kaltenpoth, M. Grunze, R. M. Penner, *J. Phys. Chem. B* **2002**, *106*, 11407.
- [26] M. P. Zach, K. Inazu, J. C. Hemminger, R. M. Penner, *Chem. Mater.* **2002**, *14*, 3206.
- [27] R. M. Penner, *J. Phys. Chem. B* **2002**, *106*, 3339.
- [28] M. P. Zach, K. H. Ng, R. M. Penner, *Science* **2000**, *290*, 2120.
- [29] Y. W. Mo, F. J. Himpsel, *Phys. Rev. B* **1994**, *50*, 7868.
- [30] T. Jung, R. Schlittler, J. K. Gimzewski, F. J. Himpsel, *Appl. Phys. A* **1995**, *61*, 467.
- [31] T. Jung, Y. W. Mo, F. J. Himpsel, *Phys. Rev. Lett.* **1995**, *74*, 1641.
- [32] A. Brodde, K. Dreps, J. Binder, C. Lunau, H. Neddermeyer, *Phys. Rev. B* **1993**, *47*, 6609.
- [33] A. Brodde, H. Neddermeyer, *Surf. Sci.* **1993**, *287*, 988.
- [34] A. Brodde, G. Wilhelmi, D. Badt, H. Wengelnik, H. Neddermeyer, *J. Vac. Sci. Technol. B* **1991**, *9*, 920.
- [35] F. J. Himpsel, T. Jung, A. Kirakosian, J. L. Lin, D. Y. Petrovykh, H. Rauscher, J. Viernow, *MRS Bull.* **1999**, *24*, 20.
- [36] F. J. Himpsel, T. Jung, J. E. Ortega, *Surf. Rev. Lett.* **1997**, *4*, 371.
- [37] D. Y. Petrovykh, F. J. Himpsel, T. Jung, *Surf. Sci.* **1998**, *407*, 189.
- [38] P. Gambardella, M. Blanc, H. Brune, K. Kuhnke, K. Kern, *Phys. Rev. B* **2000**, *61*, 2254.
- [39] H. Röder, E. Hahn, H. Brune, J.-P. Bucher, K. Kern, *Nature* **1993**, *366*, 141.
- [40] A. Dallmeyer, C. Carbone, W. Eberhardt, C. Pampuch, O. Rader, W. Gudat, P. Gambardella, K. Kern, *Phys. Rev. B* **2000**, *61*, R5133.
- [41] M. Blanc, K. Kuhnke, V. Marsico, K. Kern, *Surf. Sci.* **1998**, *414*, L964.
- [42] J. D. Noll, M. A. Nicholson, P. G. VanPatten, C. W. Chung, M. L. Myrick, *J. Electrochem. Soc.* **1998**, *145*, 3320.
- [43] M. Aktary, C. E. Lee, Y. Xing, S. H. Bergens, M. T. McDermott, *Langmuir* **2000**, *16*, 5837.
- [44] M. P. Zach, R. M. Penner, *Adv. Mater.* **2000**, *12*, 878.
- [45] C. A. Amatore, J.-M. Savéant, D. Tessier, *J. Electroanal. Chem.* **1983**, *147*, 39.
- [46] C. A. Amatore, M. R. Deakin, R. M. Wightman, *J. Electroanal. Chem.* **1986**, *207*, 23.
- [47] C. A. Amatore, B. Fosset, M. R. Deakin, R. M. Wightman, *J. Electroanal. Chem.* **1987**, *225*, 33.
- [48] C. A. Amatore, B. Fosset, *Anal. Chem.* **1996**, *68*, 4377.

Received: September 11, 2002 [C508]